The Arabidopsis "retrovirome" and its regulation by epigenetically activated small RNA

Seung Cho Lee[1,3], Evan Ernst[1,3], Benjamin Berube[2], Filipe Borges[1], Andrea Schorn[2], Jean-Sebastien Parent[1], Paul Ledon[2], Robert A. Martienssen[1, 2*]

[1] Howard Hughes Medical Institute, Cold Spring Harbor Laboratory, 1 Bungtown Road, Cold Spring Harbor, NY 11724, USA

[2] Cold Spring Harbor Laboratory, 1 Bungtown Rd, Cold Spring Harbor, NY 11724, USA

[3] These authors contributed equally

[*] Correspondence: martiens@cshl.edu

Running title: The Arabidopsis retrovirome and its regulation

Abstract

In Arabidopsis, LTR-retrotransposons are activated by mutations in the chromatin remodeler DECREASE in DNA METHYLATION 1 (DDM1), giving rise to 21-22nt epigenetically activated siRNAs (easiRNAs). We purified virus-like-particles (VLPs) from *ddm1* and *ddm1rdr6* mutants in which genomic RNA is reverse transcribed into complementary DNA. Next generation short-read and long-read sequencing of VLP DNA (VLP DNA-seq) revealed a comprehensive catalog of active LTR-retrotransposons without the need for mapping transposition, and independent of genomic copy number. Linear replication intermediates of *ATCOPIA93*/*EVADE* revealed multiple central polypurine tracts (cPPT), a feature shared with HIV where cPPT promote nuclear localization. For *ATCOPIA52*, cPPT intermediates were not observed, but abundant circular DNA indicated transposon "suicide" by auto-integration within the VLP. easiRNA targeted *ATCOPIA93*/*EVADE* genomic RNA, polysome association of *GYPSY* (*ATHILA*) subgenomic RNA, and transcription via histone H3 lysine-9 dimethylation. VLP DNA-seq provides a comprehensive landscape of LTR-retrotransposons, and their control at transcriptional, post-transcriptional and reverse transcriptional levels.

Introduction

Long terminal repeat (LTR) retrotransposons are a major component of the large genomes of most animal and plant species (Huang et al., 2012; Wang et al., 2014). However, the relative activity of any individual element can only be assessed using transposition assays, or by comparing insertion sites among individuals within a population. The mouse genome, for example, contains more than one million endogenous retroviruses, of which only a handful are autonomous elements. We have developed an alternative strategy for retrotransposon discovery, using next generation sequencing of replication intermediates from viral-like particles (VLP). By sequencing intermediates from different genetic backgrounds, insights can be gained into mechanisms of genetic and epigenetic regulation.

VLPs have been isolated in yeast and Drosophila (Bachmann et al., 2004; Eichinger and Boeke, 1988; Kenna et al., 1998) as well as in plants (Bachmair et al., 2004; Jaaskelainen et al., 1999). Ty1/Copia elements in plants have a single open reading frame that encodes both the GAG protein, which is the capsid protein responsible for VLP formation, and the reverse transcriptase, RNase H, and integrase polyprotein (POL) which are co-assembled with their genomic RNA (gRNA) into VLPs (Finnegan, 2012; Pachulska-Wieczorek et al., 2016; Peterson-Burch and Voytas, 2002; Sabot and Schulman, 2006). Ty3/gypsy elements also have a single GAG-POL ORF, although the POL proteins are in a different order. In yeast, Ty1 uses a frameshift between GAG and POL to enhance translation of GAG. In both Drosophila and plants, the Ty1/copia GAG protein is translated from an abundant, alternatively spliced subgenomic RNA (Chang et al., 2013; Yoshioka et al., 1990). In Arabidopsis Ty1/copia elements, the subgenomic *GAG* RNA is more efficiently translated than unspliced GAG-POL transcripts, and blocking splicing leads to significant reduction of GAG protein translation (Oberlin et al., 2017). After VLP formation in the cytoplasm, LTR retrotransposons proliferate through tRNA-primed reverse transcription of gRNA, followed by nuclear import of cDNA and integration into new loci (Schorn and Martienssen, 2018) (Supplemental Fig. S1). In yeast and Arabidopsis, tRNA-iMet initiates reverse transcription of the LTR from the primer binding site (PBS) to the 5' end of the R region making minus-strand strong-stop DNA (Griffiths et al., 2018; Mules et al., 1998; Schorn and Martienssen, 2018). RNase H degrades the template RNA upstream of the PBS, and minus-strand strong-stop DNA is transferred to the 3' LTR to prime minus strand cDNA synthesis toward the PBS (Supplemental Fig. S1). During the extension of minus-strand cDNA synthesis, the template RNA is degraded except for an RNase H-resistant polypurine tract (PPT) near the 3' LTR (Wilhelm et al., 2001). This PPT RNA fragment primes plus-strand strong-stop DNA synthesis up to U5 and the PBS sequence from the translocated minus strand (Supplemental Fig. S1B). Then, the plus-strand cDNA is transferred to the 5' end to prime full length double-stranded DNA. Additional central PPT (cPPT) can also initiate plus-strand synthesis which is displaced by the 3' end of plus-strand DNA causing DNA flaps to form during Ty1 replication (Garfinkel et al.,

2006). cPPT and DNA flaps have been found in the highly active lentivirus HIV-1 where they play roles in nuclear import and in preventing mutagenesis by APOBEC (Hu et al., 2010; VandenDriessche et al., 2002; Wurtzer et al., 2006; Zennou et al., 2000).

Inhibition of retrotransposons by small RNA has been reported in metazoans and plants, as well as in fission yeast, and occurs at the transcriptional and post-transcriptional levels. In Drosophila, piwi-interacting RNA (piRNA) trigger transcriptional silencing of transposons in the germline (Czech et al., 2018) resembling fission yeast in this respect (Volpe et al., 2002). By contrast, *Ago2* and *Dcr2* lie in the post-transcriptional pathway, and mutations result in increased somatic retrotransposition (Xie et al., 2013). In mammalian embryos, 3' tRNA fragments (3'-tRF) control transposition of LTR retrotransposons both post-transcriptionally and by direct inhibition of reverse transcription (Schorn et al., 2017). In Arabidopsis, transcriptional activation of some LTR retrotransposons by stress, or by loss of histone methylation, also requires loss of 24nt small RNA and RDR2/RNA polymerase IV (Ito et al., 2011; Mirouze et al., 2009). By contrast, in *ddm1* mutants and wild-type pollen, most transposons are transcriptionally activated and 24nt siRNA are partly replaced by 21-22nt easiRNA (Slotkin et al., 2009). In *ddm1* mutants, easiRNA are generated by RDR6 (Creasey et al., 2014; Nuthikattu et al., 2013) from the non-functional *ATHILA2* and *ATHILA6* Ty3/gypsy retrotransposons but also from the functional, TY1/copia element *EVADE*, and are triggered by diverse miRNA. In wild-type, retroelements generate easiRNA only in pollen, where they are targeted at the PBS by miR845, and biogenesis occurs via a non-canonical pathway (Borges et al., 2018).

In order to develop a comprehensive catalog of functional retrotransposons in Arabidopsis, we performed VLP DNA sequencing from *ddm1* mutants, as well as genome-wide polysomal RNA (translatome) and chromatin immunoprecipitation (ChIP) sequencing. VLP sequencing recovered all known active retrotransposons in Arabidopsis, without the need for genome sequencing of

transposition events. Replication intermediates revealed profound differences between elements with multiple cPPT and high integration rates, and elements with no cPPT which preferentially integrated into themselves ("suicidal" auto-integration within the VLP). We examined the roles of easiRNA in retrotransposon control by investigating *ddm1rdr6* double mutants (Creasey et al., 2014; Lippman et al., 2004; Vongs et al., 1993). We found that some retrotransposons are regulated post-transcriptionally by RNA interference, while others are regulated at the transcriptional level by histone H3 lysine-9 methylation guided by small RNA. We conclude that easiRNA inhibits retrotransposition at multiple levels in the replication cycle and identify features of active retrotransposons that promote activity and escape from silencing.

Results

Characterization of functional LTR retrotransposons by VLP DNA sequencing

Functional LTR retrotransposons form VLPs assembled from GAG proteins (Sabot and Schulman, 2006) (Supplemental Fig. S1A). Reverse transcription occurs inside the VLPs, and cDNA products are subsequently imported into the nucleus bound to the integrase protein. After integration into new genomic loci these insertions transcribe additional gRNA. We purified VLPs after treatment with DNase I (Methods), and sequenced cDNA products from wild-type, *ddm1,* and *ddm1rdr6* using both short read (Illumina) and long read (Oxford Nanopore Technologies) sequencing platforms (Supplemental Fig. S2). *EVADE* is one of two full length elements of the *ATCOPIA93* family in *A. thaliana* Col-0, and when it is transcriptionally activated, it is the most successful retroelement by far in terms of copy number increases, although transposition of *ATGP3*, *ATCOPIA13*, *ATCOPIA21, ATCOPIA31*, *ATCOPIA51*, *ATCOPIA63*, *ATGP2N*, and *ATRE1* have also been detected under non-stressed conditions (Ito et al., 2011; Quadrana et al., 2019; Tsukahara et al., 2009). Full length VLP DNA from all of these elements was dramatically enriched in *ddm1* and *ddm1rdr6* mutants consistent with active reverse transcription (Fig. 1; Supplemental Figs. S2,S3; Supplemental Table S1). VLP DNA from some *ATCOPIA* families

were more enriched in *ddm1* than *ddm1rdr6*, likely due to transcriptional down-regulation in *ddm1rdr6* (Creasey et al., 2014). VLP DNA from *ATHILA* families were enriched in *ddm1rdr6*, but comprised small fragments, mostly from the LTR likely reflecting abortive retrotransposition intermediates from these non-functional elements (Supplemental Fig. S3A) (Marco and Marin, 2008). By contrast, long read coverage of *EVADE* and other active *COPIA* elements spanned the entire element, and was increased in *ddm1rdr6* (Fig. 1B; Supplemental S2B; Supplemental Table S1). Furthermore, linear extrachromosomal DNA (ecDNA) was dramatically increased in *ddm1rdr6* by Southern blot (Fig. 2A).

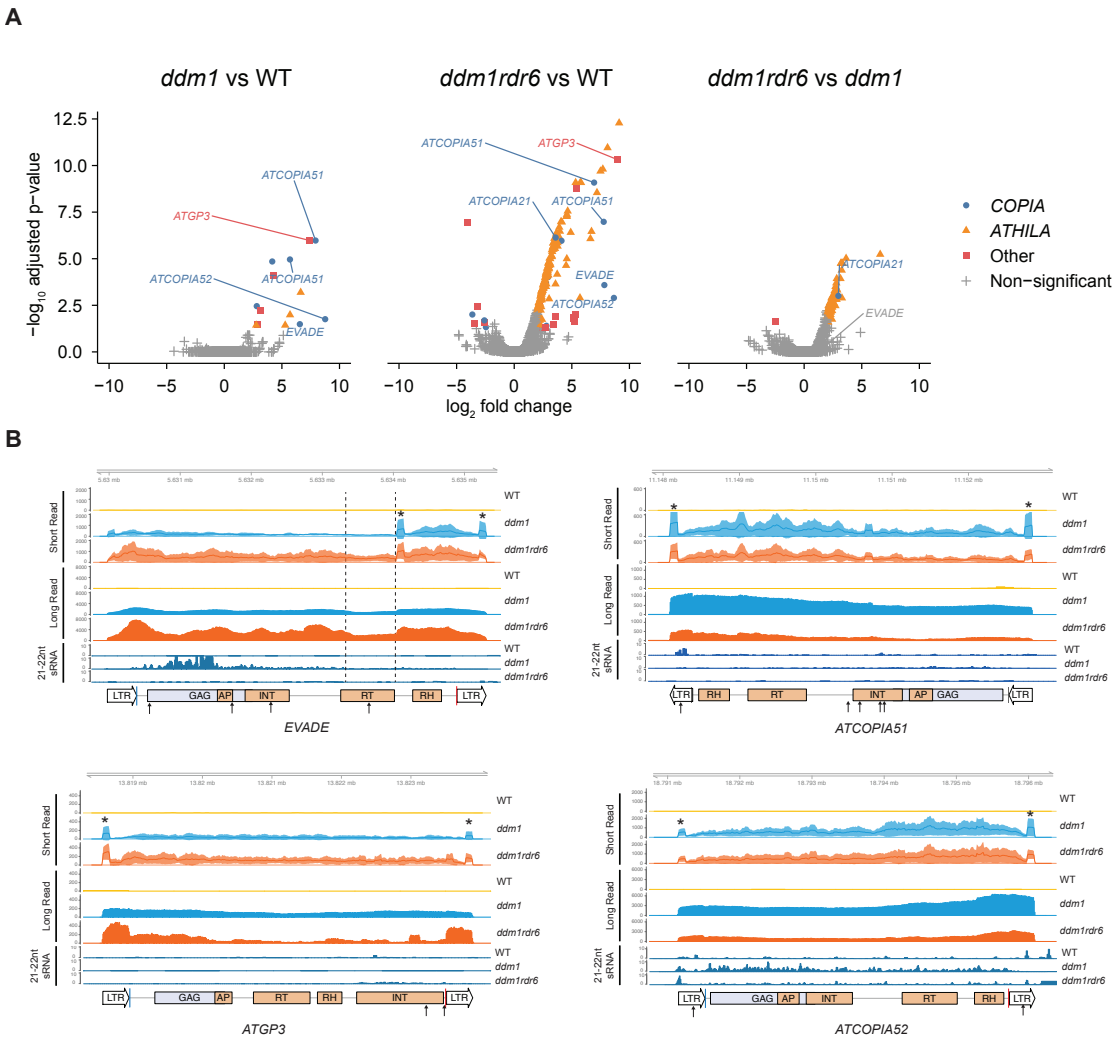

Figure 1. VLP DNA-seq data of LTR retrotransposons in *ddm1* and *ddm1rdr6*. (A) Differential analysis of paired-end sequencing of VLP DNA using Illumina short read platform. The statistical significance of three comparisons of wild-type (WT), *ddm1*, and *ddm1rdr6* is shown with $|\log_2$ (fold

change)| ≥ 2 and FDR threshold at 5%. Each point corresponds to an annotated transposable element. Multiple *ATHILA* families were combined and labeled as '*ATHILA*'. (B) Coverage of short and long read VLP DNA-seq at representative LTR retrotransposon loci (*EVADE*, AT5TE20395; *ATGP3*, AT1TE45315; *ATCOPIA51*, AT1TE36035; *ATCOPIA52*, AT3TE76225) were plotted for *ddm1* and *ddm1rdr6*. Mean read counts per million mapped reads and 95% confidence intervals of biological replicates are shown for WT (yellow, n=3), *ddm1* (blue, n=2), and *ddm1rdr6* (orange, n=3) short read libraries. VLP DNA replicate samples were pooled for each genotype and sequenced in aggregate by Oxford Nanopore long read sequencing. In the LTR retrotransposon annotation, abbreviations for conserved protein domains within the GAG-POL ORF are indicated as GAG, AP (amino peptidase), INT (integrase), RT (reverse transcriptase), and RH (RNase H). Blue and red lines indicate primer binding sites (PBS) and polypurine tracts (PPT). 21-22nt small RNA (sRNA) data were obtained from a previous study (Creasey et al., 2014). Target positions of miRNAs are indicated as arrows (see Supplemental Table S4 for details). Central PPT (cPPT) positions are indicated as dashed lines. Elevated coverage at the edges of strong-stop intermediate and flap DNA is shown as asterisks above *ddm1* short read data.

cDNA can exist in both linear and circular forms, and circular forms were previously reported for *EVADE* and other members of the *ATCOPIA93* family (Lanciano et al., 2017; Reinders et al., 2013). We observed outward-facing paired-end read alignments from Illumina VLP-seq samples mapping to *ATCOPIA51*, *ATCOPIA52*, *EVADE*, and *ATGP3*, consistent with junction-crossing reads from circular templates (Fig. 2B). Outward-facing pairs appeared in the *ddm1* and *ddm1rdr6* samples, but not in WT, and were present in very low numbers after read de-duplication for most of the elements. Exceptionally, non-concordant read pairs were highly abundant in *ATCOPIA52*. Circular ecDNA formation was confirmed by inverse PCR whose products corresponded to one-LTR in size (Fig. 2C,D), and *ATCOPIA52* was by far the most abundant. Double stranded one-LTR circular products are thought to be generated by integrase-mediated autointegration in VLP, or as gapped intermediates in cDNA synthesis (Garfinkel et al., 2006; Munir et al., 2013; Sloan and Wainberg, 2011). In contrast, two-LTR (tandem) circular DNA with junction nucleotides is formed in the nucleus by non-homologous end joining and enhanced when integrase is non-functional (Garfinkel et al., 2006; Sloan and Wainberg, 2011). The inverse PCR products of *ATCOPIA52* were one-LTR in size, suggesting the circular DNA was either a gapped double stranded circular intermediate, or else a double stranded product of

autointegration into same strands or opposite strands (Supplemental Fig. S1), which result in deletion circles, or inversion circles, respectively (Garfinkel et al., 2006; Munir et al., 2013; Sloan and Wainberg, 2011). Both inversion and deletion circles were detected in large numbers based on outward facing reverse-forward and forward-forward paired end reads, respectively, indicating auto-integration was the major source of these circles (Fig. 2B).

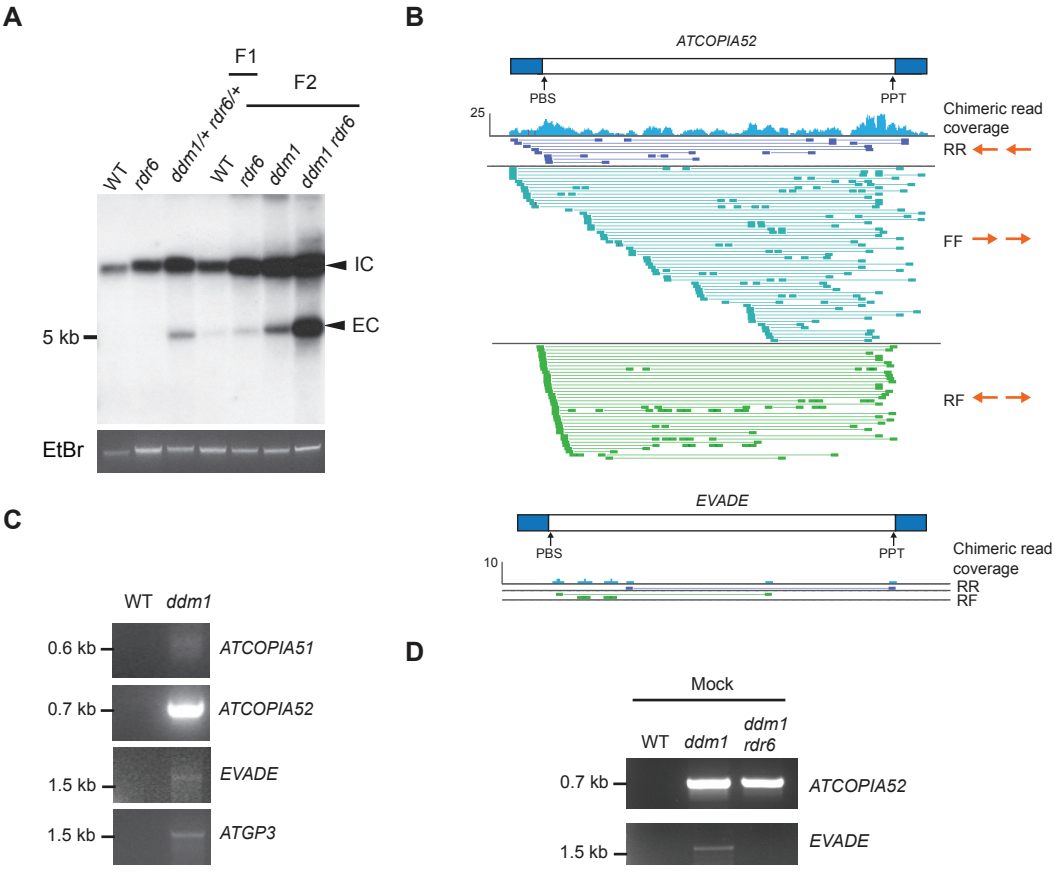

Figure 2. Extrachromosomal DNA of LTR retrotransposons in *ddm1* and *ddm1rdr6*. (A) Southern blotting using an *EVADE* probe was performed with undigested genomic DNA of F1 and F2 plants from the same parental lines. Integrated DNA copies (IC) and extrachromosomal DNA copies (EC) are indicated. Ethidium Bromide (EtBr) staining was used for loading control. (B) Discordant short read alignments from *ATCOPIA52* (AT3TE76225) and *EVADE* in *ddm1*. Read pair orientations (forward or reverse for the first and second mate): RR and FF reads align in the same direction to the reference, indicating inversions, while RF reads face outward, indicating circular templates. LTR regions are indicated as blue bars. (C) Inverse PCR with genomic DNA to detect circular extrachromosomal DNA from *ATCOPIA51*, *ATCOPIA52*, *EVADE*, and *ATGP3* in *ddm1* plants. (D) Inverse PCR with VLP DNA and reverse-forward (RF) outward reading primers for *ATCOPIA52* and *EVADE*. (C-D) PCR primers are listed in Supplemental Table S6.

In yeast, auto-integration occurs near the central PPT (cPPT) taking advantage of a DNA flap structure (Garfinkel et al., 2006). There was no strong indication of a DNA flap based on polypurine sequences and read alignment in *ATCOPIA52*. We mapped individual long reads to investigate the integration sites (Fig. 3; Supplemental Figs. S1C, S3B). Deletion circles are predicted to have either the 5' or the 3' LTR, as well as a deleted portion of the full length cDNA, up to the integration site, while inversion circles have an inverted portion separating the two LTR (Garfinkel et al., 2006). Strikingly, many of the *ATCOPIA52* ONT reads fell into these categories, comprising either the 5' or the 3' LTR contiguous with a truncated or inverted portion of the retrotransposon (Supplemental Fig. S1C). These structural variants indicated the presence of circularly permuted reads, which were presumably arbitrarily sheared during library preparation. Among all the *COPIA* and *GYPSY* elements examined, only *ATCOPIA52* gave rise to large numbers of these structural variants. The inversions spanned diverse regions of the element, consistent with inversion circles. The deleted portions terminated at inferred autointegration sites, which were distributed throughout the length of the element, consistent with the lack of a cPPT flap in *ATCOPIA52*. One possibility is that nuclear import of cDNA is not efficient for *ATCOPIA52,* leading to elevated autointegration inside the VLP. This could be due to mutations in nuclear localization (Kenna et al., 1998), or else to reduced translation of the integrase gene (see below), although read distributions were comparable for *ddm1* and *ddm1rdr6*, so easiRNA likely did not play a major role.

In sharp contrast, in *EVADE* we observed discontinuous regions of read alignments flanked by multiple cPPT, defined as 15-19 nt polypurine sequences (Figs. 1B,3; Supplemental Fig. S3B). These regions represent active replication intermediates, generated by both minus strand and plus strand strong stop DNA, as well as extension products that terminate at cPPT and DNA flaps. The numbers of these intermediates, as well as their abundance, were significantly elevated in long-read sequencing data from *ddm1rdr6* double mutants (Figs. 1B,3; Supplemental Fig. S3B). *ATGP3* also had elevated levels of strong stop intermediates, but few if any cPPT and no circular

206 reads.

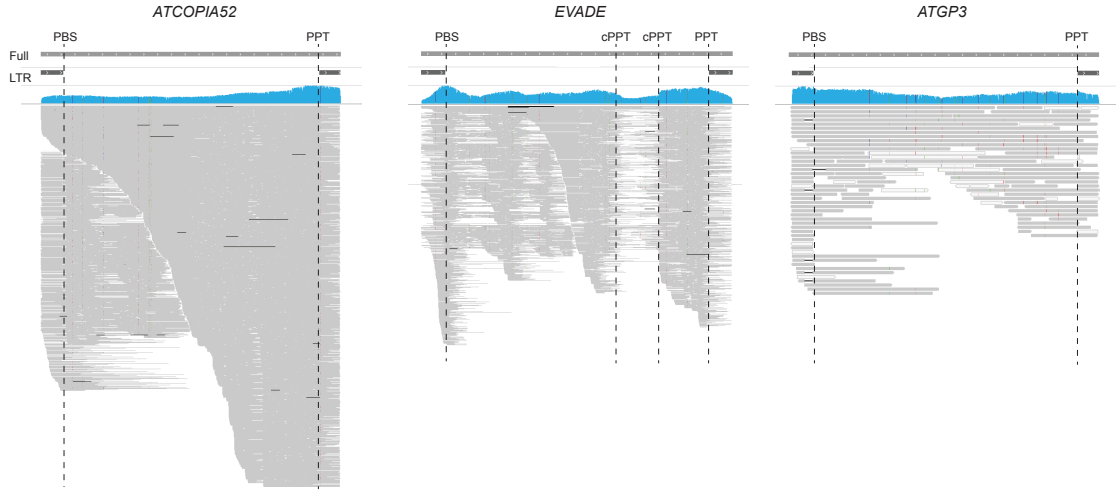

207

208 **Figure 3. Alignments of Oxford Nanopore long reads from *ddm1* VLP DNA.** The central polypurine
209 tract (cPPT), PBS, and PPT positions are indicated as dashed lines relative to full and LTR annotation of
210 *ATCOPIA52* (AT3TE76225), *EVADE* (AT5TE20395), and *ATGP3* (AT1TE45315). Gaps in individual
211 reads are indicated with black horizontal lines, and sequence mismatches are shown as colored dots in the
212 read alignments. Pileups of linear intermediates are observed for *EVADE*, while a continuous distribution
213 of fragment lengths is observed in *ATCOPIA52*.

214

215 **21-22nt easiRNA control retrotransposition**

216 In a previous study, DCL2/4 were shown to promote transcription of *EVADE* transgenes driven
217 by an ectopic promoter, while RDR6 had no effect, which was interpreted as evidence that
218 easiRNA might promote transposition in wild-type cells (Mari-Ordonez et al., 2013). We tested
219 whether easiRNA contribute to *EVADE* control in *ddm1* and *ddm1rdr6* mutants. Both *ddm1* and
220 *ddm1rdr6* contained higher copy numbers of *ATCOPIA93* than wild-type implying high rates of
221 *EVADE* transposition, while copy numbers of *ATGP3* and *ATCOPIA52* remained constant. Using
222 quantitative PCR, we detected an increase from 2 copies of *EVADE* in wild-type to 12 copies in
223 *ddm1* to 40 copies in *ddm1rdr6* F2 siblings (Fig. 4A). Similar increases were observed in F2 and
224 F3 progeny from backcross *rdr6* progeny that inherited active *EVADE* elements epigenetically

225 (Fig. 4C) (Mari-Ordonez et al., 2013). We detected parallel increases in gRNA levels reflecting
226 these increases in copy number (Fig. 4B,D). Consistent with gRNA levels, extrachromosomal
227 *EVADE* copies were also more abundant in *ddm1rdr6* than in *ddm1* (Fig. 2A). RNase H cleavage
228 products just upstream of the PBS, which are a hallmark of active transposition (Schorn et al.,
229 2017), were readily detected for *EVADE* in both *ddm1* and *ddm1rdr6* (Supplemental Fig. S4A,B).
230 We conclude that easiRNA actually inhibit *EVADE* retrotransposition, in *ddm1* mutants.

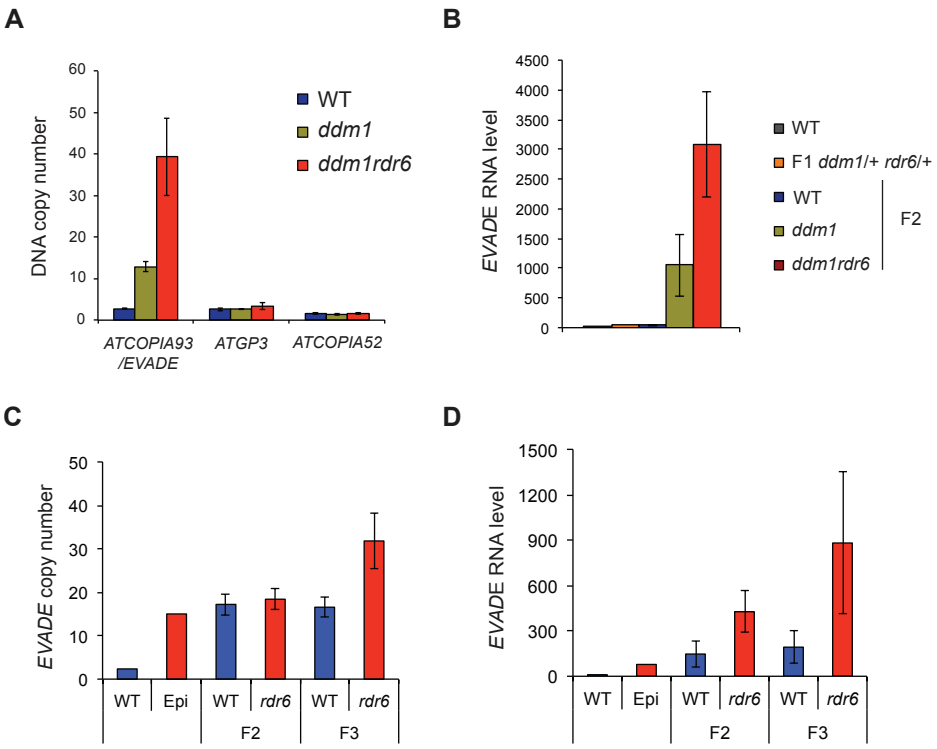

231

232 **Figure 4. DNA and RNA levels of LTR retrotransposons in *ddm1* and *rdr6* mutants.** (A) DNA copy
233 numbers of *ATCOPIA93*, *ATGP3*, and *ATCOPIA52* in *ddm1* and *ddm1rdr6* were normalized with a single
234 copy gene (AT5G13440). (B) RT-qPCR data of *EVADE* elements using POL primers. Y-axis indicates
235 relative levels of *EVADE* genomic RNA to wild-type (WT) after normalization to *ACT2*. (C-D) *EVADE*
236 DNA copy number and genomic RNA levels were analyzed in F2 and F3 progenies of F1 plants carrying
237 active *EVADE* epigenetically inherited from parental *rdr6*/+ (Epi) crossed with WT pollen. Error bars
238 indicate standard deviations (n=3).

239

240 In backcrosses to wild-type (WT) plants, *EVADE* activity is inherited epigenetically but copy

number increases are thought to be limited by a switch from 21nt to 24nt siRNA, accompanied by re-methylation and silencing (Mari-Ordonez et al., 2013; Mirouze et al., 2009; Reinders et al., 2013). Interestingly, active *EVADE* elements can be re-silenced through the female gametophyte, but not through the male gametophyte (Reinders et al., 2013) where easiRNA normally accumulate (Borges et al., 2018; Slotkin et al., 2009). We sequenced small RNA from wild type and *ddm1* flower buds and pollen, and found that 21-22nt easiRNA from *ATCOPIA93*/*EVADE* were abundant in *ddm1* inflorescence tissues, but absent from pollen (Fig. 5). In contrast, *ATHILA2* and *ATHILA6A* easiRNA were present in wild type pollen (Slotkin et al., 2009), while *ATCOPIA31* 21-22nt easiRNA were strongly upregulated in *ddm1* pollen. Thus the absence of *EVADE* easiRNA in pollen must be due to transcriptional repression independent of DDM1, and likely accounts for the lack of paternal re-silencing (Reinders et al., 2013).

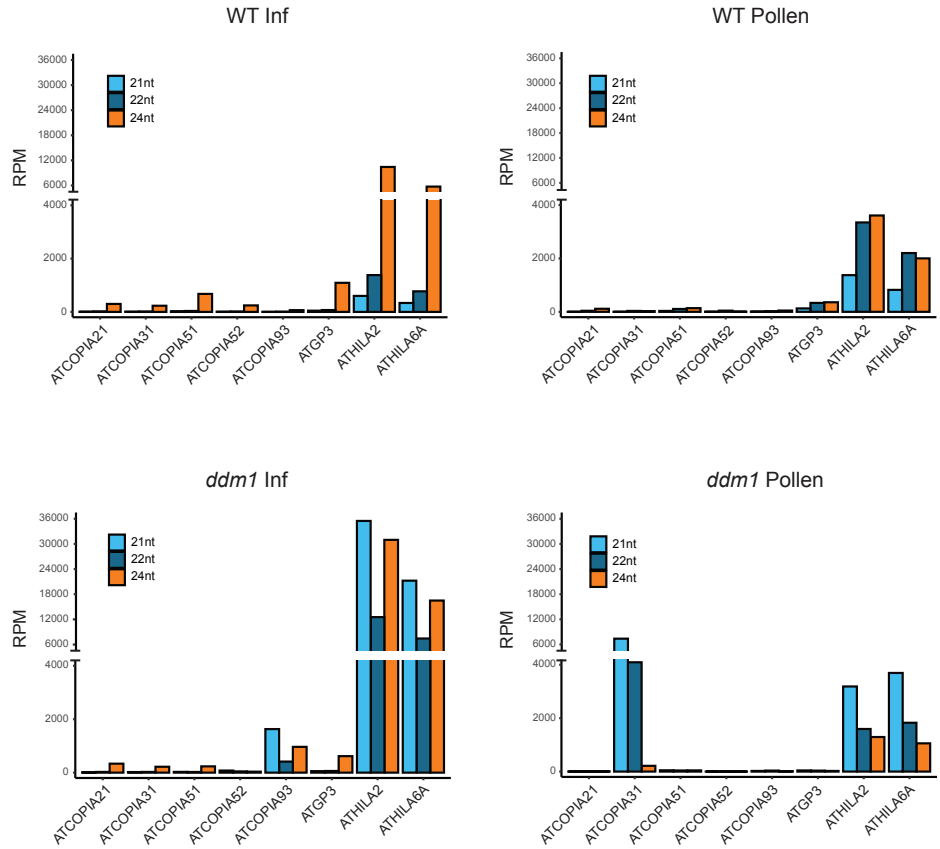

Figure 5. Small RNA profiles of representative LTR retrotransposons. 21, 22, and 24nt small RNA levels in inflorescence tissues and pollen of wild-type (WT) and *ddm1*. Reads per million (RPM) was

255 calculated from entire elements including LTR and coding sequences.

256

257 **Post-transcriptional suppression by easiRNA**

258 Since easiRNA in *ddm1* mutants depend on AGO1 (Nuthikattu et al., 2013), and AGO1 represses
259 translation of target mRNA (Li et al., 2013), we tested whether easiRNA can affect translation
260 efficiency of transposon transcripts. Translating ribosome affinity immunopurification (TRAP)
261 RNAseq has been utilized to estimate polysomal occupancy and translation efficiency in plants
262 (Juntawong et al., 2014). Furthermore, microsome-polysomal fractionation has revealed that
263 microRNA-dependent translational control takes place on the endoplasmic reticulum (Li et al.,
264 2013). We generated TRAP lines of *35S:FLAG-RPL18* in *ddm1* and *ddm1rdr6* mutant
265 backgrounds, and performed total RNAseq, total-polysomal RNAseq, and microsome-polysomal
266 RNAseq. The polysomal RNA occupancy (Polysomal RNA / Total RNA) was obtained for 3903
267 transposable elements defined as open reading frames from TAIR10 annotation (see Methods).
268 As for the comparison between *ddm1* and *ddm1rdr6*, we could detect the effect of the *rdr6*
269 mutation in microsome-polysomal RNAseq data for known targets of RDR6, such as *ARF4*
270 (Marin et al., 2010), and for a handful of transposons (Fig. 6A; Supplemental Fig. S5;
271 Supplemental Tables S2,S3). Among 31 up-regulated transposons in *ddm1rdr6* relative to *ddm1*,
272 26 elements belonged to *ATHILA* LTR retrotransposon families (Supplemental Table S3), which
273 are a major source of RDR6-dependent easiRNA. Although *ATHILA* elements in *A. thaliana*
274 cannot transpose, a subgenomic mRNA encoding ORF2 (the "env" gene) is spliced from the full
275 length mRNA (Havecker et al., 2004; Wright and Voytas, 2002), and was enriched on polysomes
276 (Supplemental Fig. S5; Supplemental Table S3). This subgenomic RNA is targeted extensively
277 by miRNA which trigger easiRNA production (Creasey et al., 2014). Interestingly, the other 3
278 elements were *ATENSPM3*, *LINE1_6* and *VANDAL3*, all of which have been identified as active
279 elements in *ddm1* mutants, or in population level studies of transposon variants (Stuart et al.,
280 2016). These non-LTR and DNA transposons are also targets of miRNA and generate RDR6-

dependent easiRNA (Creasey et al., 2014). *EVADE* easiRNA are generated from the GAG subgenomic RNA (Mari-Ordonez et al., 2013), but polysomal occupancy was not increased in *ddm1rdr6* (Fig. 6B). GAG subgenomic mRNA from *ATCOPIA52* was highly enriched in polysomes, consistent with previous studies (Oberlin et al., 2017), whereas the relative abundance of *EVADE* POL transcripts on polysomes indicates higher translation rates of integrase and reverse transcriptase (Oberlin et al., 2017). Unlike for *ATHILA*, polysome association of *COPIA* transcripts were unaffected by RDR6.

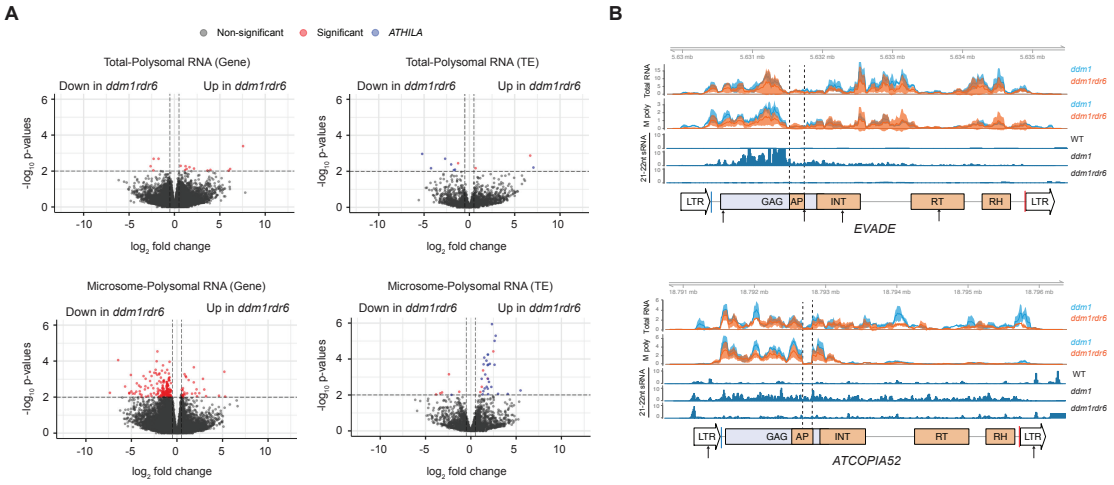

Figure 6. Translatome profiles of *ddm1* and *ddm1rdr6*. (A) Differential analysis of polysomal RNAseq data between *ddm1* and *ddm1rdr6*. Polysomal RNAseq values were normalized by total RNA seq values to reflect polysomal enrichment (Methods). Red dots indicate significantly regulated genes or transposable elements (TE) by cut-off values of $|\log_2 (\text{fold change})| > 0.5$ and p-values < 0.01 which include *ARF4* as an internal control. Significantly regulated *ATHILA* family elements are labeled with blue dots. (B) Total RNA and microsome-polysomal RNA (M poly) levels are shown for *EVADE* (*ATCOPIA93*; AT5TE20395) and *ATCOPIA52* (AT3TE76225). Mean read counts per million mapped reads and 95% confidence intervals of three biological replicates are shown for *ddm1* (blue) and *ddm1rdr6* (orange). Conserved protein domains, PBS and PPT, small RNA profiles and miRNA target sites are indicated as in Fig. 1.

easiRNA require miRNA triggers that target these transcripts (Creasey et al., 2014), and *ATCOPIA52* LTRs were targeted by a single miRNA in the R region of the LTR. Consistent with this miRNA acting as a trigger, easiRNA accumulated along the length of the mRNA between the

LTRs (Fig. 6B; Supplemental Table S4). In the case of *EVADE*, 4 miRNA were predicted to target the gRNA somewhere along its length. Remarkably, miR2938 was predicted to target the start codon of the GAG gene immediately 5' of the easiRNA cluster, while miR5648-5p targets the 3' end of the easiRNA cluster (Supplemental Fig. S4C,D; Supplemental Table S4). *EVADE* easiRNAs were down-regulated in *ddm1dcl1* as compared to *ddm1* (Supplemental Fig. S4E) suggesting that miRNA were involved (Creasey et al., 2014). miR2938 and miR5648-5p expression were reported in pollen and root cells (Breakfield et al., 2012; Grant-Downton et al., 2009). We did not detect miRNA-mediated cleavage by PARE-seq (Creasey et al., 2014) or by RACE-PCR, but secondary siRNA, such as easiRNA, do not require cleavage so long as miRNA recognition recruits RdRP (Axtell et al., 2006; de Felippes et al., 2017). Consistent with induction without cleavage, *EVADE* easiRNA were not phased (Arribas-Hernandez et al., 2016). miR5663 was detected in inflorescence tissues (Supplemental Fig. S4F), and targets the *EVADE* intron near the splice acceptor site (Supplemental Fig. S4C). Interestingly, the level of unspliced RNA was increased in *ddm1dcl1* mutants (Supplemental Fig. S4G), indicating that miR5663 might target unspliced gRNA and promote the accumulation of spliced GAG RNA, but further experiments would be required to demonstrate this requirement. Negative regulation of *P*-element splicing by piRNA has been reported in Drosophila (Teixeira et al. 2017). *ATCOPIA21* and *ATCOPIA51* had no strongly predicted miRNA targets, and easiRNA were barely detected in somatic tissues (Fig. 1B; Supplemental Fig. S3A) (Oberlin et al., 2017) accounting for lack of regulation by *RDR6*. In contrast, significant levels were detected in pollen (Fig. 5) (Borges et al., 2018), where most gypsy and copia class retrotransposons are targeted by miR845, a pollen specific miRNA that targets the primer binding site (Borges et al., 2018).

Transcriptional repression by easiRNA

Both 21/22nt easiRNA and especially 24nt siRNA can direct RNA directed DNA methylation in plants, via AGO6 and AGO4, respectively (Borges and Martienssen, 2015). However, genome

wide bisulphite sequencing revealed few if any differences in DNA methylation between *ddm1* and *ddm1rdr6*, as *ddm1* mutants already had very low levels of DNA methylation (Creasey et al., 2014). In many organisms, histone modification can also be guided by small RNA, especially histone H3 lysine-9 dimethylation (Fagegaltier et al., 2009; Gu et al., 2012; Martienssen and Moazed, 2015; Volpe et al., 2002). We therefore performed H3K9me2 ChIP sequencing in *ddm1* and *ddm1rdr6*, and compared this to wild type. We found that *ATHILA* elements, which matched by far the most abundant easiRNA, had ectopic H3K9me2 in *ddm1* mutants, which was absent in *ddm1rdr6* mutants (Fig. 7; Supplemental Fig. S6). Furthermore, the levels of small RNA correlated extremely well with the levels of H3K9me2 found at individual *ATHILA* elements (Fig. 7; Supplemental Fig. S6). Interestingly, *COPIA* elements actually gained H3K9me2 in the absence of easiRNA (Supplemental Fig. S7), along with previously reported increases in 24nt siRNA and reduced transcript levels (Creasey et al., 2014). We therefore conclude that in the absence of DDM1, 21/22nt easiRNA and 24nt siRNA can guide H3K9me2 at *GYPSY* and *COPIA* elements respectively.

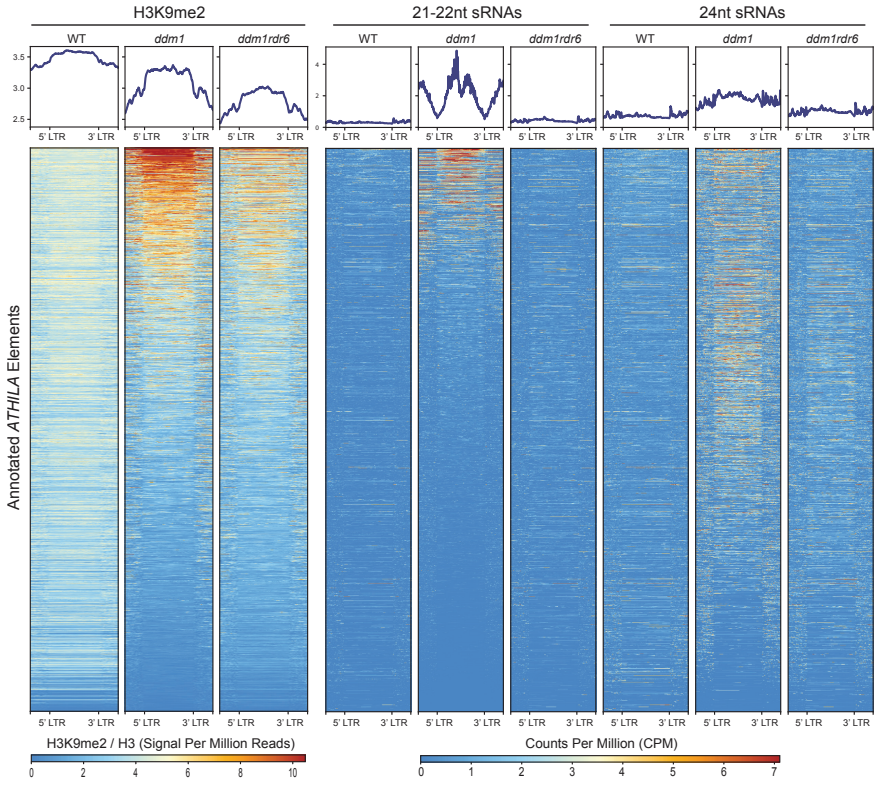

Figure 7. *ATHILA* family elements gain RDR6-dependent H3K9me2 in *ddm1*. H3K9me2 signal at transposable elements from multiple *ATHILA* families was analyzed in wild-type (WT), *ddm1*, and *ddm1rdr6* genotypes and correlated with previously published small RNA data (Creasey et al., 2014). RDR6-dependent gains in H3K9me2 co-localize with increased 21-22nt siRNAs in *ddm1*. Plots depict transposable elements annotations scaled to 5kb, as well as 2kb upstream and downstream of each feature. H3K9me2 ChIP data was normalized by H3, and small RNA data was normalized by counts per million.

Discussion

Next generation sequencing of VLP DNA detected all known functional LTR retrotransposons in Arabidopsis, as well as some non-functional ones. Full length VLP DNA from *ATCOPIA* and *ATGP* families (Fig. 1B; Supplemental Fig. S3A) corresponded to relatively young and low-copy elements known to transpose. Ancient *ATHILA* elements did not make full length VLP DNA confirming these gypsy retrotransposons are non-functional (Havecker et al., 2004; Marco and Marin, 2008), but short products matching the LTR appeared to correspond to aborted strong stop replication intermediates (Supplemental Fig. S3A). Interestingly, similar LTR fragments from *ATHILA2* comprise an important family of dispersed centromeric satellite repeats known as 106B (May et al., 2005; Thompson et al., 1996), and retrotransposition might account for their origin. Thus functional and non-functional retrotransposons could be readily distinguished even though non-functional *ATHILA* elements are present in copy numbers 3 to 4 orders of magnitude higher than active *ATCOPIA* and *ATGP* elements. As for *ATCOPIA52*, non-productive one-LTR circular DNA, corresponding to autointegration "suicide" products, markedly accumulated in the VLP at levels far higher than productive retrotransposons such as *EVADE*. In contrast, two-LTR circular products of *ATCOPIA52* were very rare, whereas small amounts of *EVADE* two-LTR products were present as previously described (Reinders et al., 2013), presumably due to recombination of non-integrated copies by host DNA repair enzymes in the nucleus. Both short read and long read sequencing revealed that these auto-integration products in *ATCOPIA52* VLP led to non-functional deletion and inversion circles, accounting for lack of transposition.

Our study shows that RDR6-dependent easiRNA inhibit retrotransposition at multiple levels: via post-transcriptional silencing of genomic RNA, by translational suppression of subgenomic RNA, and by controlling transcription via histone modification. *ATHILA* elements are no longer functional, but they are the primary source of easiRNA which arise by miRNA targeting of a spliced subgenomic RNA encoding the "ENV" protein (Creasey et al., 2014). These easiRNA inhibit polysome association of this subgenomic RNA, and also inhibit transcript levels by guiding histone H3K9me2. This transcriptional silencing occurred in the absence of DNA methylation in *ddm1* mutants. In plants, RNAi dependent histone modification is thought to depend entirely on RNA dependent DNA methylation, found in asymmetric CHH contexts. As CHH methylation stays more or less the same in *ddm1*, while H3K9me2 is increased (Fig. 7), this might indicate the existence of a novel pathway for RNA guided histone methylation, resembling that found in Drosophila, *C.elegans* and fission yeast, which lack DNA methylation. Further investigation will be required to establish if such a pathway exists.

In contrast to *ATHILA*, linear extrachromosomal copies of *EVADE* accumulated in *ddm1* and were further enriched by mutations in *RDR6*. Like *ATHILA*, *EVADE* is targeted by 3 or 4 miRNA that likely trigger easiRNA from the subgenomic GAG gene transcript, which is found associated with polysomes (Oberlin et al., 2017). However, association of the GAG mRNA with polysomes was unaffected in *ddm1rdr6* mutants. Instead, levels of gRNA increased 3-fold, suggesting that *EVADE* easiRNA act postranscriptionally to target gRNA directly. *ATCOPIA52* easiRNA arose from full-length gRNA between the two LTR. Polysomal association of full length *EVADE* GAG-POL is far more abundant than *ATCOPIA52* GAG-POL, although both were unchanged in the absence of *RDR6* (Fig. 6). As the INT protein is translated from this transcript, this could contribute to lack of nuclear integration of *ATCOPIA52* relative to *EVADE*. Thus, while easiRNA have a significant impact on *COPIA* gRNA accumulation, and so inhibit increases in copy number, they have only limited impact on translation. 22nt tRNA-derived small RNA fragments (3'CCA-tRFs) were recently shown to inhibit endogenous retroviruses (ERV) in mammalian cells

by targeting the PBS by RNA interference (Schorn et al., 2017), and it is possible that *EVADE* easiRNA may have a similar function in plants.

In conclusion, next generation long-read and short-read sequencing of VLP DNA has revealed features that distinguish functional and non-functional replication intermediates, and provides a powerful tool for identifying active transposons from complex genomes, and for investigating molecular signatures of LTR retrotransposons. One such feature is the central PPT (cPPT), which is present in *EVADE* but absent in *ATCOPIA52*. cPPT are hallmarks of the most active retrotransposons including Ty1 in yeast, as well as HIV and other lentiviruses, where cPPT are thought to be important for nuclear import of cDNA (VandenDriessche et al., 2002; Zennou et al., 2000). Our work shows that these features may play a significant role in the activity of *EVADE*, the most active retrotransposon in Arabidopsis, and that their absence may account for the lack of nuclear integration of *ATCOPIA52*, and high levels of "suicide" by autointegration. By comparing VLP sequencing, transcriptome sequencing and translatome sequencing we have been able to establish the multiple levels at which easiRNA regulate the Arabidopsis retrovirome. Our methods are widely applicable to other plant and animal models and to human cells, especially those with genomes that contain very large numbers of non-functional LTR retrotransposons.

Acknowledgements

We thank Vincent Colot, Leandro Quadrano, Tetsuji Kakutani and all members of the Martienssen laboratory for discussions. Research in the Martienssen laboratory is supported by the US National Institutes of Health (NIH) grant R01 GM067014, The National Science Foundation Plant Genome Research Program, and by the Howard Hughes Medical Institute. The authors acknowledge assistance from the Cold Spring Harbor Laboratory Shared Resources, which are funded in part by the Cancer Center Support Grant (5PP30CA045508).

Author Contributions

SCL, EE and RM designed the study; SCL and EE performed the experiments; SCL, EE, BB, and AS analyzed the data and its significance; SCL, EE and RM wrote the manuscript.

Disclosure declaration

The authors declare no competing interest.

Methods

Plant materials

All genotypes in this study are Col-0 background including wild-type, *dcl1-11*, *ddm1-2*, and *rdr6-15*. Genotyping primers are listed in Supplemental Table S6. Homozygous plants of *ddm1-2* and *ddm1-2 rdr6-15* were generated from heterozygous *ddm1-2* backcrossed five times with Col-0 (*ddm1-2* BC5), and their 2nd generation was used for VLP DNA-seq experiments. For polysomal RNAseq experiments, inbred *ddm1-2* was independently crossed to *35S:FLAG-RPL18* and to *rdr6-15 35S:FLAG-RPL18*. The F3 plants were used for polysomal RNA purification.

gDNA extraction and DNA analyses

Whole inflorescence stems of 4 week-old Arabidopsis plants were frozen and ground in liquid nitrogen. Total gDNA was isolated using Nucleon PhytoPure kit (GE healthcare). *EVADE* DNA copy number was quantified using qPCR with *EVADE* qPCR primers and single copy gene primers as reference (the primers are listed in Supplemental Table S6). Southern blotting was performed using *EVADE* Probe B as described (Mirouze et al., 2009).

445 **Chromatin immunoprecipitation (ChIP)**

446 ChIP was performed with two biological replicates of 10-d-old seedlings using H3K9me2
447 (Abcam; ab1220) and H3 (Abcam; ab1791) antibodies, following a previously described protocol
448 (Ingouff et al., 2017). Sequencing libraries were prepared using NEBNext Ultra II DNA Library
449 Prep Kit for Illumina (New England Biolabs) with size selection for ~200 bp insert DNA. The
450 ChIP-seq libraries were sequenced using Illumina NextSeq High Output SR 76 with 76-cycle
451 single reads. Two biological replicates were prepared and sequenced for each genotype of interest.
452 Prior to alignment, adapter trimming was performed using Trimmomatic (Bolger, et al., 2014)
453 and read quality was assessed with FastQC
454 (http://www.bioinformatics.babraham.ac.uk/projects/fastqc). Reads were aligned to the TAIR10
455 reference genome using BWA-MEM (https://arxiv.org/abs/1303.3997) with default parameters.
456 Only primary alignments were retained, and optical and PCR duplicates were removed using
457 Samtools (Li et al., 2009). Peak calling was performed using MACS2 (Zhang et al., 2008) broad
458 peak calling with a q-value cutoff of 0.05 and normalization by signal per million reads. Peaks
459 that were differentially regulated across genotypes were identified using MAnorm (Shao et al.,
460 2012) and confirmed between biological replicates. Annotation of these differentially regulated
461 peaks was performed using a combination of BEDOPS (Neph et al., 2012) tools and custom
462 scripts. Deeptools (Ramirez et al., 2014) was used to visualize the data.

463

464 **RNA extraction and RT-qPCR**

465 Total RNA was isolated from the same tissues used for gDNA extraction with Direct-zol RNA
466 MiniPrep Plus (Zymo Research). DNase I was treated on column. cDNA was synthesized with
467 SuperScript VILO Master Mix (Thermo Fisher Scientific). qPCR was performed using iQ SYBR
468 Green Supermix. Primers are listed in Supplemental Table S6.

469

Polysomal RNA-seq

Total polysome was isolated using ribosome immunopurification as described previously (Mustroph et al., 2009; Mustroph et al., 2013). Briefly, inflorescence tissues of *FLAG-RPL18* lines were ground in liquid nitrogen and transferred to polysome extraction buffer (PEB). Cell debris was removed by centrifugation and filtering with miracloth. The supernatant was taken and transferred to pre-washed EZview anti-FLAG agarose beads (Sigma) for 2 h at 4 °C. The agarose beads containing polysomes were washed once with PEB and three times with washing buffer. Polysomes were eluted using 3X FLAG peptide (Sigma) and used for RNA extraction with Direct-zol RNA miniprep kit (Zymo Research) including DNase I treatment. Ribosomal RNA (rRNA) in the samples was depleted by Ribo-Zero Magnetic Kit (Plant Leaf) (Epicentre). Then, rRNA free samples were used for RNA-seq library preparation using ScriptSeq v2 RNA-Seq Library Preparation Kit (EPicentre). Microsome-polysomal RNA was obtained using a previously described method with some modifications (Li et al., 2013). Briefly, 2 g frozen tissues were suspended to 7 ml microsome extraction buffer (MEB). After removing cell debris by filtration with micracloth and centrifugation at 10,000g for 15 min at 4°C, the supernatant was transferred on the top of 1.7M/0.6M sucrose cushions and applied to ultracentrifugation using swing rotor at 140,000g for 1 h at 4°C. The microsome fraction of the 1.7M/0.6M layer interface was harvested and diluted 10 times by MEB and centrifuged at 140,000g for 0.5 h at 4 °C to obtain microsome pellet. The pellet was re-suspended with 8 ml PEB and used for ribosome immunopurification and RNA-seq library preparation as described above. The PE 101 sequencing data was obtained using Illumina HiSeq 2000 platform. The paired-end reads were mapped to Arabidopsis TAIR10 genome using Tophat and the polysome occupancy (Polysomal RNA / Total RNA) was calculated using systemPipeR package (Backman and Girke, 2016) with raw count data obtained by Cuffnorm.

VLP DNA-seq

Virus-like-particles were purified using modified method reported previously (Bachmair et al., 2004). 4 g of 4 week-old whole inflorescence stems were ground with 10 ml of ice-cold VLP extraction buffer and 10 ml of sea sand on ice. 10 ml of the extraction buffer and Triton X-100 were added and mixed. The slurry was transferred to a 50 ml tube and centrifuged for 5 min at 180g and 4 °C. The supernatant was carefully transferred onto 5 ml of prechilled 15% sucrose, 10 mM potassium phosphate buffer, pH 7.2 and ultracentrifuged for 1.5 h at 109,000g and 4 °C using fixed angle rotor. The pellet was washed with the 15% sucrose buffer and resuspended with 4 ml particle suspension buffer to obtain VLP fractions. To remove non-VLP DNA, 0.5 ml of the VLP sample was treated with 5 µl of 1 mg/ml DNase I at 37°C for 10 min. 20 µl of 0.25 M EDTA, 50 µl of 10% SDS, 25 µl of 10 mg/ml proteinase were added and incubated at 65°C for 10 min. VLP DNA was purified by 0.5 ml equilibrated (pH 8.0) phenol:chloroform:IAA (25:24:1) mixture three times and with 0.5 ml chloroform:IAA (24:1) once. The last aqueous fraction was transferred into a new 1.5ml tube and used for 100% ethanol precipitation with 40 µl 3M sodium acetate, pH 7.0. The DNA pellet was washed with 70% ethanol, dried, and resuspended with 100 µl TE buffer. 1 µl of RNase A (10 mg/ml) was added to the VLP DNA sample and incubated 10 min. The treated DNA sample was purified using DNA Clean & Concentrator (Zymo Research). The DNA was sheared to 650 bp using Covaris S220 and subsequently used for DNA-seq library preparation with NEBNext Ultra DNA Library Prep Kit (New England Biolabs). The paired-end sequencing datasets with 101 nt read length (PE101) were obtained by Illumina HiSeq 2000. Adapters were trimmed from raw reads with Skewer (Jiang et al., 2014) in paired-end mode and read pairs with both mates longer than 25 nt were retained. Reads were aligned to the TAIR10 genome with STAR (Dobin et al., 2013) in two-pass mode to improve spliced alignment at unannotated introns. Intact bacteria co-purified with VLP, as indicated by large numbers of reads mapping to bacterial genomes (up to 95% in WT), and these were discarded. Reads mapping equally well to multiple locations were randomly assigned, and chimeric/split read alignments were output separately from concordant alignments. Optical and PCR duplicates were removed

from the alignments with picard-tools (http://broadinstitute.github.io/picard). Counts of reads mapping to the TAIR10 transposon annotations were computed with featurecounts (Liao et al., 2014). Pairwise differential expression at TAIR10 transposon loci was tested across three wild-type, two *ddm1*, and three *ddm1rdr6* replicates using quasi-likelihood F-tests in edgeR (Robinson et al., 2010), controlling FDR at 5% and a $\log_2$(fold-change) threshold of 2.

Oxford Nanopore Technologies (ONT) long-read libraries were prepared as follows: 10 ng per genotype of purified VLP DNA extract was pooled from the replicate samples and initially amplified following the conditions in the "1D Low-input genomic DNA with PCR" (SQK-LSK108) protocol with reagents. End-repair, dA-tailing and PCR adapter ligation were performed, followed by 16 cycles of PCR amplification. PCR products were purified and concentrated with Ampure XP beads (Agencourt), and 300 ng of eluate per sample was carried through to library preparation following the "1D Genomic DNA by Ligation" protocol with SKQ-LSK109 reagents. Libraries were loaded onto r9.4 (FLO-MIN106) flow cells and sequenced on a GridION X5. Basecalling was performed offline with Guppy v2.3.1 using the default r9.4.1 model. Using porechop (https://github.com/rrwick/Porechop), ONT sequencing adapters were trimmed from 5' ends, 3' ends, and the middle of raw reads. Reads with middle adapters were split. Remaining reads longer than 100 bp were aligned to the TAIR10 reference with minimap2 (Li, 2018) for coverage and read alignment plots. Structural variants were called on NGMLR (Sedlazeck et al., 2018) alignments using Sniffles (Sedlazeck et al., 2018) with default parameters, except minimum read support was reduced to 3.

5' RACE PCR

5' RACE PCR was performed using FirstChoice RLM-RACE Kit (Thermo Fisher Scientific) without the treatments of calf intestine alkaline phosphatase and tobacco acid pyrophosphatase. A

548 gene-specific primer was used for cDNA synthesis after adaptor ligation (Supplemental Table S6).
549 1st and 2nd nested PCR was performed with the primers are listed.

550

551 **Small RNA-seq data**

552 Small RNA-seq libraries from inflorescence and pollen for comparisons of 21, 22, and 24nt small
553 RNA between wild-type and *ddm1* were prepared as previously described (Borges et al., 2018).
554 Wild-type pollen sample was previously deposited in the Gene Expression Omnibus (GEO)
555 database (GSM2829912). Briefly, small RNAs were purified by running total RNA from pollen
556 and inflorescence tissues on acrylamide gels (15% polyacrylamide, 7 M urea) with size-selection
557 of 18-to- 30-nt regions. Small RNAs were extracted from the gel bands using Trizol LS (Life
558 Technologies) and Direct-zol columns (Zymo Research). Libraries were prepared with the
559 TruSeq small RNA sample preparation kit (Illumina) and sequenced in Illumina MiSeq platform.
560 Data analysis was done as previously reported (Borges et al., 2018). 21-22nt small RNA datasets
561 from inflorescence (Creasey et al., 2014) were obtained from NCBI GEO accession GSE52951.
562 After adapter trimming with Skewer, reads were quality filtered with fastp (Chen et al., 2018) and
563 aligned to the TAIR10 genome with ShortStack (Axtell, 2013) with default parameters except "--
564 bowtie_m 1000 --ranmax 50".

565

566 **LTR Retrotransposon Annotation**

567 GenomeTools was used to structurally annotate retrotransposons across the TAIR10 genome.
568 First, LTRharvest (Ellinghaus et al., 2008) was run to detect LTR sequences with at least 85%
569 similarity separated by 1-15 kbp flanked by target site duplications and the TGCA motif. Then,
570 LTRdigest (Steinbiss et al., 2009) was run to annotate internal transposon features including the
571 PBS, PPT, and GAG and POL protein homology.

572

573 **Genome Browser Figures**

574 Genome-wide read coverage for VLP DNA, small RNA, total and polysomal RNA libraries was
575 calculated with bamCoverage from deepTools (Ramirez et al., 2014) and normalized to reads per
576 nucleotide per million mapped reads and plotted across the genome with Gviz (Hahne and Ivanek,
577 2016) or IGV (Thorvaldsdottir et al., 2013).

578

579 **Data access**

580 The datasets generated during and/or analyzed during the current study are available at NCBI
581 (GEO study: GSE128932).

582

583 **References**

584 Arribas-Hernandez L, Marchais A, Poulsen C, Haase B, Hauptmann J, Benes V, Meister G,
585 Brodersen P. 2016. The Slicer Activity of ARGONAUTE1 Is Required Specifically for the
586 Phasing, Not Production, of Trans-Acting Short Interfering RNAs in Arabidopsis. *Plant Cell* **28:**
587 1563-1580.

588

589 Axtell MJ. 2013. ShortStack: comprehensive annotation and quantification of small RNA genes.
590 *RNA* **19:** 740-751.

591

592 Axtell MJ, Jan C, Rajagopalan R, Bartel DP. 2006. A two-hit trigger for siRNA biogenesis in
593 plants. *Cell* **127:** 565-577.

594

595 Bachmair A, Garber K, Takeda S, Sugimoto K, Kakutani T, Hirochika H. 2004. Biochemical
596 analysis of long terminal repeat retrotransposons. *Methods Mol Biol* **260:** 73-82.

597

598 Bachmann AS, Corpuz G, Hareld WP, Wang G, Coller BA. 2004. A simple method for the rapid
599 purification of copia virus-like particles from Drosophila Schneider 2 cells. *J Virol Methods* **115:**
600 159-165.
601
602 Backman T, Girke T. 2016. systemPipeR: NGS workflow and report generation environment.
603 *BMC Bioinformatics* **17:** 388.
604
605 Bolger AM, Lohse M, Usadel B. 2014. Trimmomatic: a flexible trimmer for Illumina sequence
606 data. *Bioinformatics* **30**: 2114-2120.
607
608 Borges F, Martienssen RA. 2015. The expanding world of small RNAs in plants. *Nat Rev Mol*
609 *Cell Biol* **16:** 727-741.
610
611 Borges F, Parent JS, van Ex F, Wolff P, Martinez G, Kohler C, Martienssen RA. 2018.
612 Transposon-derived small RNAs triggered by miR845 mediate genome dosage response in
613 Arabidopsis. *Nat Genet* **50:** 186-192.
614
615 Breakfield NW, Corcoran DL, Petricka JJ, Shen J, Sae-Seaw J, Rubio-Somoza I, Weigel D, Ohler
616 U, Benfey PN. 2012. High-resolution experimental and computational profiling of tissue-specific
617 known and novel miRNAs in Arabidopsis. *Genome Res* **22:** 163-176.
618
619 Chang W, Jaaskelainen M, Li SP, Schulman AH. 2013. BARE retrotransposons are translated and
620 replicated via distinct RNA pools. *PLoS One* **8:** e72270.
621
622 Chen S, Zhou Y, Chen Y, Gu J. 2018. fastp: an ultra-fast all-in-one FASTQ preprocessor.
623 *Bioinformatics* **34:** i884-i890.
624

625 Creasey KM, Zhai J, Borges F, Van Ex F, Regulski M, Meyers BC, Martienssen RA. 2014.
626 miRNAs trigger widespread epigenetically activated siRNAs from transposons in Arabidopsis.
627 *Nature* **508:** 411-415.
628
629 Czech B, Munafo M, Ciabrelli F, Eastwood EL, Fabry MH, Kneuss E, Hannon GJ. 2018. piRNA-
630 Guided Genome Defense: From Biogenesis to Silencing. *Annu Rev Genet* **52:** 131-157.
631
632 Dai X, Zhuang Z, Zhao PX. 2018. psRNATarget: a plant small RNA target analysis server (2017
633 release). *Nucleic Acids Res* **46:** W49-W54.
634
635 de Felippes FF, Marchais A, Sarazin A, Oberlin S, Voinnet O. 2017. A single miR390 targeting
636 event is sufficient for triggering TAS3-tasiRNA biogenesis in Arabidopsis. *Nucleic Acids Res* **45:**
637 5539-5554.
638
639 Dobin A, Davis CA, Schlesinger F, Drenkow J, Zaleski C, Jha S, Batut P, Chaisson M, Gingeras
640 TR. 2013. STAR: ultrafast universal RNA-seq aligner. *Bioinformatics* **29:** 15-21.
641
642 Eichinger DJ, Boeke JD. 1988. The DNA intermediate in yeast Ty1 element transposition
643 copurifies with virus-like particles: cell-free Ty1 transposition. *Cell* **54:** 955-966.
644
645 Ellinghaus D, Kurtz S, Willhoeft U. 2008. LTRharvest, an efficient and flexible software for de
646 novo detection of LTR retrotransposons. *BMC Bioinformatics* **9:** 18.
647
648 Fagegaltier D, Bouge AL, Berry B, Poisot E, Sismeiro O, Coppee JY, Theodore L, Voinnet O,
649 Antoniewski C. 2009. The endogenous siRNA pathway is involved in heterochromatin formation
650 in Drosophila. *Proc Natl Acad Sci* **106:** 21258-21263.
651

652 Finnegan DJ. 2012. Retrotransposons. *Curr Biol* **22:** R432-437.

653

654 Garfinkel DJ, Stefanisko KM, Nyswaner KM, Moore SP, Oh J, Hughes SH. 2006.
655 Retrotransposon suicide: formation of Ty1 circles and autointegration via a central DNA flap. *J*
656 *Virol* **80:** 11920-11934.

657

658 Grant-Downton R, Le Trionnaire G, Schmid R, Rodriguez-Enriquez J, Hafidh S, Mehdi S, Twell
659 D, Dickinson H. 2009. MicroRNA and tasiRNA diversity in mature pollen of *Arabidopsis*
660 *thaliana*. *BMC Genomics* **10:** 643.

661

662 Griffiths J, Catoni M, Iwasaki M, Paszkowski J. 2018. Sequence-Independent Identification of
663 Active LTR Retrotransposons in Arabidopsis. *Mol Plant* **11:** 508-511.

664

665 Gu SG, Pak J, Guang S, Maniar JM, Kennedy S, Fire A. 2012. Amplification of siRNA in
666 *Caenorhabditis elegans* generates a transgenerational sequence-targeted histone H3 lysine 9
667 methylation footprint. *Nat Genet* **44:** 157-164.

668

669 Hahne F, Ivanek R. 2016. Visualizing Genomic Data Using Gviz and Bioconductor. *Methods Mol*
670 *Biol* **1418:** 335-351.

671

672 Havecker ER, Gao X, Voytas DF. 2004. The diversity of LTR retrotransposons. *Genome Biol* **5:**
673 225.

674

675 Hu C, Saenz DT, Fadel HJ, Walker W, Peretz M, Poeschla EM. 2010. The HIV-1 central
676 polypurine tract functions as a second line of defense against APOBEC3G/F. *J Virol* **84:** 11981-
677 11993.

678

679 Huang CR, Burns KH, Boeke JD. 2012. Active transposition in genomes. *Annu Rev Genet* **46:**
680 651-675.
681
682 Ingouff M, Selles B, Michaud C, Vu TM, Berger F, Schorn AJ, Autran D, Van Durme M,
683 Nowack MK, Martienssen RA, et al. 2017. Live-cell analysis of DNA methylation during sexual
684 reproduction in Arabidopsis reveals context and sex-specific dynamics controlled by
685 noncanonical RdDM. *Genes Dev* **31:** 72-83.
686
687 Ito H, Gaubert H, Bucher E, Mirouze M, Vaillant I, Paszkowski, J. 2011. An siRNA pathway
688 prevents transgenerational retrotransposition in plants subjected to stress. *Nature* **472:** 115-119.
689
690 Jaaskelainen M, Mykkanen AH, Arna T, Vicient CM, Suoniemi A, Kalendar R, Savilahti H,
691 Schulman AH. 1999. Retrotransposon BARE-1: expression of encoded proteins and formation of
692 virus-like particles in barley cells. *Plant J* **20:** 413-422.
693
694 Jiang H, Lei R, Ding SW, Zhu S. 2014. Skewer: a fast and accurate adapter trimmer for next-
695 generation sequencing paired-end reads. *BMC Bioinformatics* **15:** 182.
696
697 Juntawong P, Girke T, Bazin J, Bailey-Serres J. 2014. Translational dynamics revealed by
698 genome-wide profiling of ribosome footprints in Arabidopsis. *Proc Natl Acad Sci* **111:** E203-212.
699
700 Kenna MA, Brachmann CB, Devine SE, Boeke JD. 1998. Invading the yeast nucleus: a nuclear
701 localization signal at the C terminus of Ty1 integrase is required for transposition in vivo. *Mol*
702 *Cell Biol* **18:** 1115-1124.
703
704 Lanciano S, Carpentier MC, Llauro C, Jobet E, Robakowska-Hyzorek D, Lasserre E, Ghesquiere
705 A, Panaud O, Mirouze M. 2017. Sequencing the extrachromosomal circular mobilome reveals

706 retrotransposon activity in plants. *PLoS Genet* **13:** e1006630.

707

708 Li H. 2018. Minimap2: pairwise alignment for nucleotide sequences. *Bioinformatics* **34:** 3094-
709 3100.

710

711 Li H, Handsaker B, Wysoker A, Fennell T, Ruan J, Homer N, Marth G, Abecasis G, Durbin R,
712 Genome Project Data Processing S. 2009. The Sequence Alignment/Map format and SAMtools.
713 *Bioinformatics* ***25*****:** 2078-2079.

714

715 Li S, Liu L, Zhuang X, Yu Y, Liu X, Cui X, Ji L, Pan Z, Cao X, Mo B, et al. 2013. MicroRNAs
716 inhibit the translation of target mRNAs on the endoplasmic reticulum in Arabidopsis. *Cell* **153:**
717 562-574.

718

719 Liao Y, Smyth GK, Shi W. 2014. featureCounts: an efficient general purpose program for
720 assigning sequence reads to genomic features. *Bioinformatics* **30:** 923-930.

721

722 Lippman Z, Gendrel AV, Black M, Vaughn MW, Dedhia N, McCombie WR, Lavine K, Mittal V,
723 May B, Kasschau KD, et al. 2004. Role of transposable elements in heterochromatin and
724 epigenetic control. *Nature* **430:** 471-476.

725

726 Marco A, Marin I. 2008. How Athila retrotransposons survive in the Arabidopsis genome. *BMC*
727 *Genomics* **9:** 219.

728

729 Mari-Ordonez A, Marchais A, Etcheverry M, Martin A, Colot V, Voinnet O. 2013.
730 Reconstructing de novo silencing of an active plant retrotransposon. *Nat Genet* **45:** 1029-1039.

731

732 Marin E, Jouannet V, Herz A, Lokerse AS, Weijers D, Vaucheret H, Nussaume L, Crespi MD,

733 Maizel A. 2010. miR390, Arabidopsis TAS3 tasiRNAs, and their AUXIN RESPONSE FACTOR
734 targets define an autoregulatory network quantitatively regulating lateral root growth. *Plant Cell*
735 **22:** 1104-1117.
736
737 Martienssen R, Moazed, D. 2015. RNAi and heterochromatin assembly. *Cold Spring Harb*
738 *Perspect Biol* **7:** a019323.
739
740 May BP, Lippman ZB, Fang Y, Spector DL, Martienssen RA. 2005. Differential regulation of
741 strand-specific transcripts from Arabidopsis centromeric satellite repeats. *PLoS Genet* **1:** e79.
742
743 Mirouze M, Reinders J, Bucher E, Nishimura T, Schneeberger K, Ossowski S, Cao J, Weigel D,
744 Paszkowski J, Mathieu O. 2009. Selective epigenetic control of retrotransposition in Arabidopsis.
745 *Nature* **461:** 427-430.
746
747 Mules EH, Uzun O, Gabriel A. 1998. In vivo Ty1 reverse transcription can generate replication
748 intermediates with untidy ends. *J Virol* **72:** 6490-6503.
749
750 Munir S, Thierry S, Subra F, Deprez E, Delelis O. 2013. Quantitative analysis of the time-course
751 of viral DNA forms during the HIV-1 life cycle. *Retrovirology* **10:** 87.
752
753 Mustroph A, Juntawong P, Bailey-Serres J. 2009. Isolation of plant polysomal mRNA by
754 differential centrifugation and ribosome immunopurification methods. *Methods Mol Biol* **553:**
755 109-126.
756
757 Mustroph A, Zanetti ME, Girke T, Bailey-Serres J. 2013. Isolation and analysis of mRNAs from
758 specific cell types of plants by ribosome immunopurification. *Methods Mol Biol* **959:** 277-302.
759

760 Neph S, Kuehn MS, Reynolds AP, Haugen E, Thurman RE, Johnson AK, Rynes E, Maurano MT,
761 Vierstra J, Thomas S, et al. 2012. BEDOPS: high-performance genomic feature operations.
762 *Bioinformatics* **28:** 1919-1920.
763
764 Nuthikattu S, McCue AD, Panda K, Fultz D, DeFraia C, Thomas EN, Slotkin RK. 2013. The
765 initiation of epigenetic silencing of active transposable elements is triggered by RDR6 and 21-22
766 nucleotide small interfering RNAs. *Plant Physiol* **162:** 116-131.
767
768 Oberlin S, Sarazin A, Chevalier C, Voinnet O, Mari-Ordonez A. 2017. A genome-wide
769 transcriptome and translatome analysis of Arabidopsis transposons identifies a unique and
770 conserved genome expression strategy for Ty1/Copia retroelements. *Genome Res* **27:** 1549-1562.
771
772 Pachulska-Wieczorek K, Le Grice SF, Purzycka KJ. 2016. Determinants of Genomic RNA
773 Encapsidation in the Saccharomyces cerevisiae Long Terminal Repeat Retrotransposons Ty1 and
774 Ty3. *Viruses* **8:** 193.
775
776 Peterson-Burch BD, Voytas DF. 2002. Genes of the Pseudoviridae (Ty1/copia retrotransposons).
777 *Mol Biol Evol* **19:** 1832-1845.
778
779 Quadrana L, Etcheverry M, Gilly A, Caillieux E, Madoui MA, Guy J, Bortolini Silveira A,
780 Engelen S, Baillet V, Wincker P, et al. 2019. Transposition favors the generation of large effect
781 mutations that may facilitate rapid adaption. *Nat Commun* **10:** 3421.
782
783 Ramirez F, Dundar F, Diehl S, Gruning BA, Manke T. 2014. deepTools: a flexible platform for
784 exploring deep-sequencing data. *Nucleic Acids Res* **42:** W187-191.
785
786 Reinders J, Mirouze M, Nicolet J, Paszkowski J. 2013. Parent-of-origin control of

787 transgenerational retrotransposon proliferation in Arabidopsis. *EMBO Rep* **14:** 823-828.

788

789 Robinson MD, McCarthy DJ, Smyth GK. 2010. edgeR: a Bioconductor package for differential
790 expression analysis of digital gene expression data. *Bioinformatics* **26:** 139-140.

791

792 Sabot F, Schulman AH. 2006. Parasitism and the retrotransposon life cycle in plants: a
793 hitchhiker's guide to the genome. *Heredity* (Edinb) **97:** 381-388.

794

795 Schorn AJ, Gutbrod MJ, LeBlanc C, Martienssen R. 2017. LTR-Retrotransposon Control by
796 tRNA-Derived Small RNAs. *Cell* **170:** 61-71 e11.

797

798 Schorn AJ, Martienssen R. 2018. Tie-Break: Host and Retrotransposons Play tRNA. *Trends Cell*
799 *Biol* **28:** 793-806.

800

801 Sedlazeck FJ, Rescheneder P, Smolka M, Fang H, Nattestad M, von Haeseler A, Schatz MC.
802 2018. Accurate detection of complex structural variations using single-molecule sequencing. *Nat*
803 *Methods* **15:** 461-468.

804

805 Shao Z, Zhang Y, Yuan GC, Orkin SH, Waxman DJ. 2012. MAnorm: a robust model for
806 quantitative comparison of ChIP-Seq data sets. *Genome Biol* **13:** R16.

807

808 Sloan RD, Wainberg MA. 2011. The role of unintegrated DNA in HIV infection. *Retrovirology*
809 **8:** 52.

810

811 Slotkin RK, Vaughn M, Borges F, Tanurdzic M, Becker JD, Feijo JA, Martienssen RA. 2009.
812 Epigenetic reprogramming and small RNA silencing of transposable elements in pollen. *Cell* **136:**
813 461-472.

Steinbiss S, Willhoeft U, Gremme G, Kurtz S. 2009. Fine-grained annotation and classification of de novo predicted LTR retrotransposons. *Nucleic Acids Res* **37:** 7002-7013.

Stuart T, Eichten SR, Cahn J, Karpievitch YV, Borevitz JO, Lister R. 2016. Population scale mapping of transposable element diversity reveals links to gene regulation and epigenomic variation. *Elife* **5:** e20777.

Teixeira FK, Okuniewska M, Malone CD, Coux R-X, Rio DC, Lehmann R. 2017. piRNA-mediated regulation of transposon alternative splicing in soma and germline. *Nature* **552:** 268-272.

Thompson HL, Schmidt R, Dean C. 1996. Identification and Distribution of Seven Classes of Middle-Repetitive DNA in the *Arabidopsis Thaliana* Genome, *Nucleic Acids Res* **24:** 3017-3022.

Thorvaldsdottir H, Robinson JT, Mesirov JP. 2013. Integrative Genomics Viewer (IGV): high-performance genomics data visualization and exploration. *Brief Bioinform* **14:** 178-192.

Tsukahara S, Kobayashi A, Kawabe A, Mathieu O, Miura A, Kakutani T. 2009. Bursts of retrotransposition reproduced in Arabidopsis. *Nature* **461:** 423-426.

VandenDriessche T, Thorrez L, Naldini L, Follenzi A, Moons L, Berneman Z, Collen D, Chuah MK. 2002. Lentiviral vectors containing the human immunodeficiency virus type-1 central polypurine tract can efficiently transduce nondividing hepatocytes and antigen-presenting cells in vivo. *Blood* **100:** 813-822.

Volpe TA, Kidner C, Hall IM, Teng G, Grewal SI, Martienssen RA. 2002. Regulation of

heterochromatic silencing and histone H3 lysine-9 methylation by RNAi. *Science* **297:** 1833-1837.

Vongs A, Kakutani T, Martienssen RA, Richards EJ. 1993. *Arabidopsis thaliana* DNA methylation mutants. *Science* **260:** 1926-1928.

Wang W, Haberer G, Gundlach H, Glasser C, Nussbaumer T, Luo MC, Lomsadze A, Borodovsky M, Kerstetter RA, Shanklin J, et al. 2014. The *Spirodela polyrhiza* genome reveals insights into its neotenous reduction fast growth and aquatic lifestyle. *Nat Commun* **5:** 3311.

Wilhelm M, Uzun O, Mules EH, Gabriel A, Wilhelm FX. 2001. Polypurine tract formation by Ty1 RNase H. *J Biol Chem* **276:** 47695-47701.

Williams L, Carles CC, Osmont KS, Fletcher JC. 2005. A database analysis method identifies an endogenous trans-acting short-interfering RNA that targets the Arabidopsis ARF2, ARF3, and ARF4 genes. *Proc Natl Acad Sci* **102:** 9703-9708.

Wright DA, Voytas DF. 2002. Athila4 of Arabidopsis and Calypso of soybean define a lineage of endogenous plant retroviruses. *Genome Res* **12:** 122-131.

Wurtzer S, Goubard A, Mammano F, Saragosti S, Lecossier D, Hance AJ, Clavel F. 2006. Functional central polypurine tract provides downstream protection of the human immunodeficiency virus type 1 genome from editing by APOBEC3G and APOBEC3B. *J Virol* **80:** 3679-3683.

Xie W, Donohue RC, Birchler JA. 2013. Quantitatively increased somatic transposition of transposable elements in Drosophila strains compromised for RNAi. *PLoS One* **8:** e72163.

868 Yoshioka K, Honma H, Zushi M, Kondo S, Togashi S, Miyake T, Shiba T. 1990. Virus-like
869 particle formation of Drosophila copia through autocatalytic processing. *EMBO J* **9:** 535-541.
870
871 Zennou V, Petit C, Guetard D, Nerhbass U, Montagnier L, Charneau P. 2000. HIV-1 genome
872 nuclear import is mediated by a central DNA flap. *Cell* **101:** 173-185.
873
874 Zhang Y, Liu T, Meyer CA, Eeckhoute J, Johnson DS, Bernstein BE, Nusbaum C, Myers RM,
875 Brown M, Li W, et al. 2008. Model-based analysis of ChIP-Seq (MACS). *Genome Biol* **9:** R137.
876